

# Supporting Information

## Discrete Face-to-Face Stacking of Anthracene Inducing High-Efficiency Excimer Fluorescence in Solids via a Thermally-activated Phase Transition

Yue Shen,<sup>a</sup> Haichao Liu,<sup>a</sup> Shitong Zhang,<sup>a</sup> Yu Gao,<sup>a</sup> Bao Li,<sup>a</sup> Yan Yan,<sup>b</sup> Yongsheng Hu,<sup>c</sup> Lijuan Zhao<sup>a</sup> and Bing Yang<sup>\*a</sup>

<sup>a</sup> State Key Laboratory of Supramolecular Structure and Materials, College of Chemistry, Jilin University, Changchun, 130012, P. R. China

<sup>b</sup> State Key Laboratory of Inorganic Synthesis and Preparative Chemistry, College of Chemistry, Jilin University, Changchun, 130012, P. R. China

<sup>c</sup> State Key Laboratory of Luminescence and Applications, Changchun Institute of Optics, Fine Mechanics, and Physics, Chinese Academy of Sciences, Changchun, 130033, P. R. China

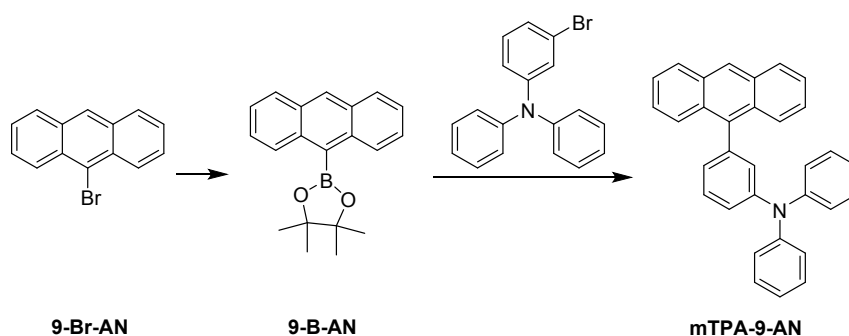
\*Corresponding Author. E-mail: [yangbing@jlu.edu.cn](mailto:yangbing@jlu.edu.cn)

## Contents

1. Synthesis of mTPA-9-AN
2. Photophysical properties
  - 2.1 Solution characters
  - 2.2 Film characters
  - 2.3 Crystal characters
3. Theoretical calculations
  - 3.1 Monomer characters
  - 3.2 Dimer characters
4. Photophysical properties of TPA-AN

## 1. Synthesis of mTPA-9-AN

*General information:* All the reagents and solvents used for the synthesis were purchased from Aldrich and Acros companies and used without further purification. The synthesis procedure was presented in Scheme S1.  $^1\text{H}$  and  $^{13}\text{C}$  NMR spectra were recorded on a Bruker AVANCE 500 spectrometer at 500 MHz, using tetramethylsilane (TMS) as the internal standard. The MALDI-TOF-MS mass spectra were recorded using an AXIMA-CFRTM plus instrument.



**Scheme S1.** Synthesis route of mTPA-9-AN

### Synthesis of 2-(anthracen-9-yl)-4,4,5,5-tetramethyl-1,3,2-dioxaborolane (9-B-AN)

A mixture of 9-Br-AN (1.02 g, 4.0 mmol), bis(pinacolato)diboron (1.52 g, 6 mmol),  $\text{PdCl}_2(\text{dppf})$  (60 mg, 0.07 mmol), KOAc (1.96 g, 20.0 mmol) and 35 mL 1, 4-dioxane was degassed and recharged with nitrogen. After stirred and refluxed at 85 °C for 48 h under nitrogen atmosphere, the mixture was washed with distilled water and then extracted with dichloromethane. The organic phase was dried with anhydrous sodium sulfate, filtered and concentrated in vacuum. The crude product was purified by passing it through a column of silica gel using petroleum ether/dichloromethane (6:1) mobile phase. The desired compound was obtained as white powder with a

60% yield (760 mg).  $^1\text{H}$  NMR (500 MHz, DMSO, 25 °C,  $\delta$ -ppm): 8.68 (s, 1H), 8.31 (d,  $J$  = 8.4 Hz, 2H), 8.11 (d,  $J$  = 8.1 Hz, 2H), 7.63 – 7.47 (m, 4H), 1.53 (s, 12H). MALDI-TOF MS (mass  $m/z$ ): 305.4 [ $M^+$ ]. Melting point: 138-140 °C.

### **Synthesis of 3-(anthracen-9-yl)-N,N-diphenylaniline (mTPA-9-AN)**

A mixture of 9-B-AN (360 mg, 1.18 mmol), 3-bromo-N,N-diphenylaniline (300 mg, 0.93 mmol),  $\text{K}_2\text{CO}_3$  (2.76 g, 20 mmol), 10 mL distilled water, 15 mL toluene and 7.5 mL anhydrous ethanol was degassed and recharged with nitrogen. Then  $\text{Pd}(\text{PPh}_3)_4$  (50 mg, 0.043 mmol) was added in the mixture as catalyst, and the mixture was degassed and recharged with nitrogen again. After stirred and refluxed at 90 °C for 24 h under nitrogen atmosphere, the mixture was extracted with dichloromethane. The organic phase was dried with anhydrous sodium sulfate, filtered and concentrated in vacuum. The crude product was purified by passing it through a column of silica gel using petroleum ether/dichloromethane (6:1) mobile phase. The desired compound was obtained as off-white powder with a 73% yield (286 mg). The product was further purified by sublimation.  $^1\text{H}$  NMR (500 MHz, DMSO, 25 °C,  $\delta$ -ppm): 8.65 (s, 1H), 8.13 (d,  $J$  = 8.4 Hz, 2H), 7.67 (d,  $J$  = 8.6 Hz, 2H), 7.58 – 7.45 (m, 5H), 7.32 (t,  $J$  = 7.9 Hz, 4H), 7.18 (m, 5H), 7.10 – 6.99 (m, 3H), 6.90 (s, 1H).  $^{13}\text{C}$  NMR (126 MHz, 25 °C  $\text{CDCl}_3$ ,  $\delta$ -ppm) 147.99, 147.78, 139.75, 136.68, 131.35, 130.03, 129.28, 129.11, 128.33, 126.79, 126.53, 125.59, 125.33, 125.08, 124.38, 122.89, 122.78. MALDI-TOF MS (mass  $m/z$ ): 421.25 [ $M^+$ ].

## **2. Photophysical properties**

*General information:* UV-vis absorption spectra of solutions were recorded on a Shimadzu UV-3100 Spectrophotometer. PL spectra of solution, film and crystal under ambient pressure were recorded with a Shimadzu RF-5301PC. Thermochromic PL spectra were measured with FLS980 Spectrometer. Fluorescence lifetimes were carried out with FLS980 Spectrometer. Quantum efficiencies were carried out on an Edinburgh FLS920 using an integrating sphere apparatus. The X-ray diffraction data was collected with a Rigaku R-Axis RAPID, and the crystal structures were solved with a SHELXTL software. Differential scanning calorimetry (DSC) analysis was carried out using a NETZSCH (DSC-204) instrument at 10 °C min<sup>-1</sup> while flushing with nitrogen.

The radiative decay rate ( $k_r$ ) and non-radiative decay rate ( $k_{nr}$ ) were calculated according to Equation 1.

$$k_r = \frac{\eta_{PL}}{\tau}, \quad k_{nr} = \frac{1}{\tau} - k_r \quad \text{.....(1)}$$

## 2.1 Solution characters

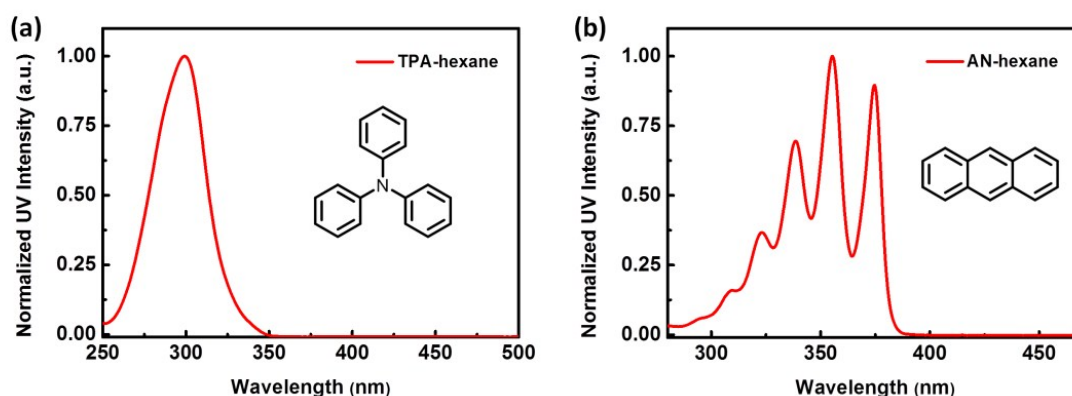


**Fig. S1** UV-vis absorption spectra of TPA and anthracene (AN) at concentration of  $\sim 10^{-5}$  M in hexane solution at room temperature.

The aggregation-induced PL spectra were examined in acetonitrile (ACN):H<sub>2</sub>O mixtures. Its emission was rather weak at the wavelength around 530 nm when the proportion of water was low, because the strong CT emissive state in high polarity solvent ACN could seriously quench fluorescence. When the water content was increased to >57 vol%, the fluorescence of the ACN/water mixture was enhanced suddenly with a hypsochromic shift to about 462 nm (Figure S2). Furthermore, the long-lived components at 500 nm were added gradually and the lifetime was extended gradually with the increase of water content (Table S1). For example, three long-lived components of 122.4 ns, 29.70 ns, 19.62 ns were detected in a ACN:H<sub>2</sub>O mixture of 5:95 (v/v). These results also indicate that the different aggregations of mTPA-9-AN form with the increase of water content in ACN:H<sub>2</sub>O mixed solvent.

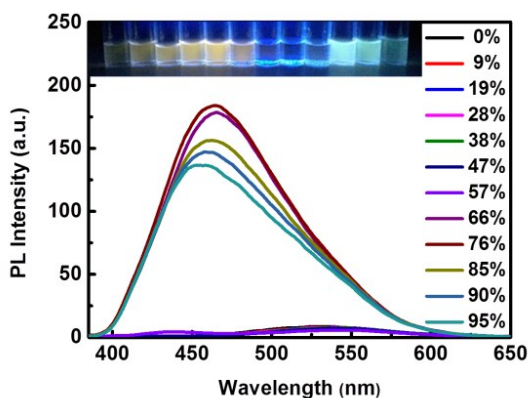


**Fig. S2** PL spectra and photograph in ACN: H<sub>2</sub>O solutions with different water content at concentration of  $\sim 10^{-5}$  M in different proportion of water.

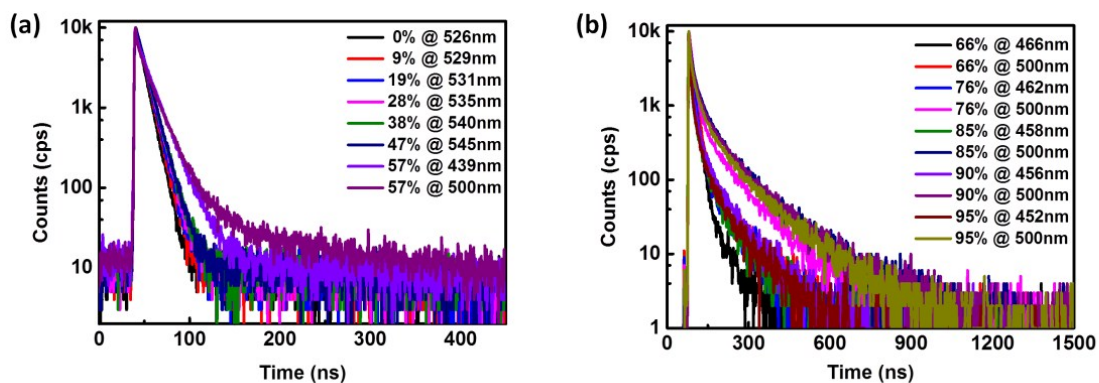


**Fig. S3** The lifetimes of ACN:H<sub>2</sub>O mixtures at concentration of  $\sim 10^{-5}$  M in different proportion of water.

**Table S1.** The lifetimes of ACN:H<sub>2</sub>O mixtures in different proportion of water

Water content (%)		$\tau_1$ (ns)	$\tau_2$ (ns)	$\tau_3$ (ns)
0		8.06	---	---
9		8.72	---	---
19		9.26	---	---
28		9.75	---	---
38		9.97	---	---
47		10.10	---	---
57	@439	2.16(4.37%)	14.74(95.63%)	---
	@500	1.62(5.54%)	14.91(94.56%)	---
66	@466	13.11(94.57%)	59.09(5.43)	---
	@500	14.09(85.47%)	80.64(14.53%)	---
76	@462	11.52(87.42%)	73.14(12.58%)	---
	@500	13.14(63.84%)	95.27(36.16%)	---
85	@458	4.29(35.01%)	19.89(47.46%)	85.50(17.53%)
	@500	8.65(21.34%)	35.41(42.93%)	128.9(35.73%)
90	@456	4.56(29.22%)	20.27(48.68%)	90.50(22.11%)
	@500	7.08(18.46%)	32.43(43.68%)	129.1(37.86%)
95	@452	4.37(34.28%)	17.82(44.21%)	79.13(21.51%)
	@500	6.32(19.62%)	29.70(41.92%)	122.4(38.47%)

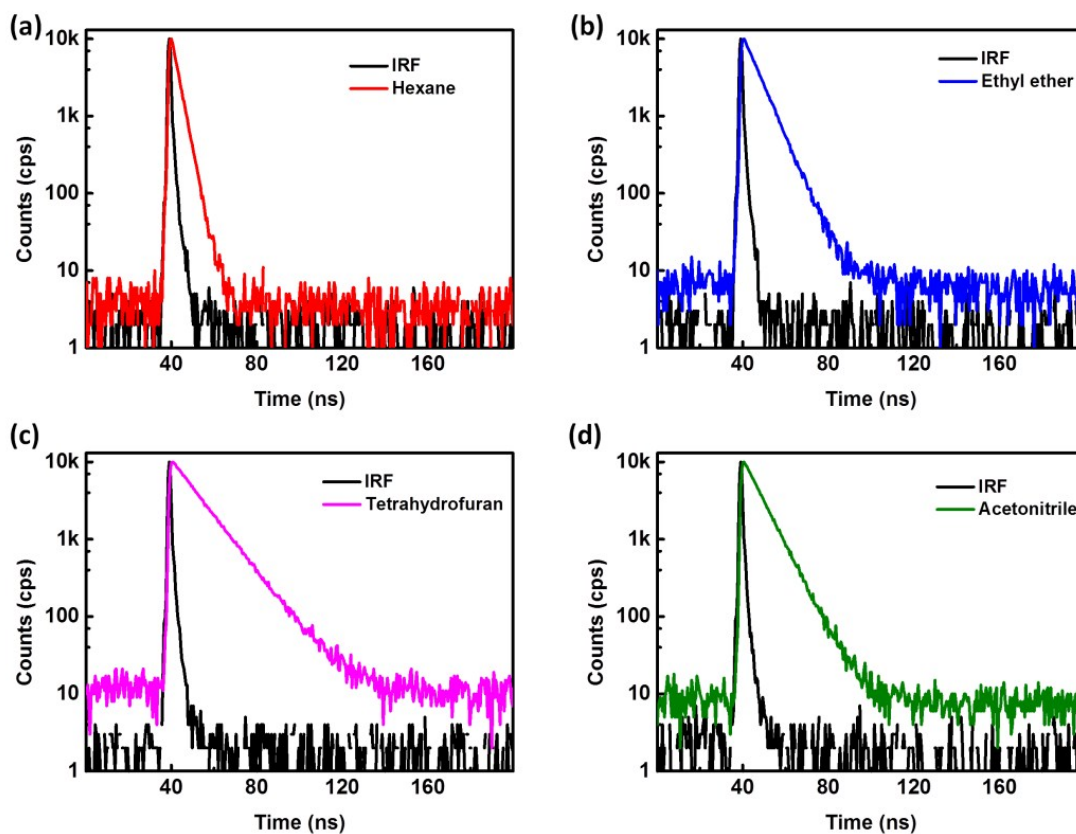


**Fig. S4** The lifetimes of mTPA-9-AN solution at concentration of  $\sim 10^{-5}$  M in (a) hexane ( $\tau = 3.04$  ns), (b) ethyl ether ( $\tau = 6.69$  ns), (c) tetrahydrofuran ( $\tau = 12.06$  ns), (d) ACN ( $\tau = 7.85$  ns). IRF represents the instrumental response function.

## 2.2 Film characters

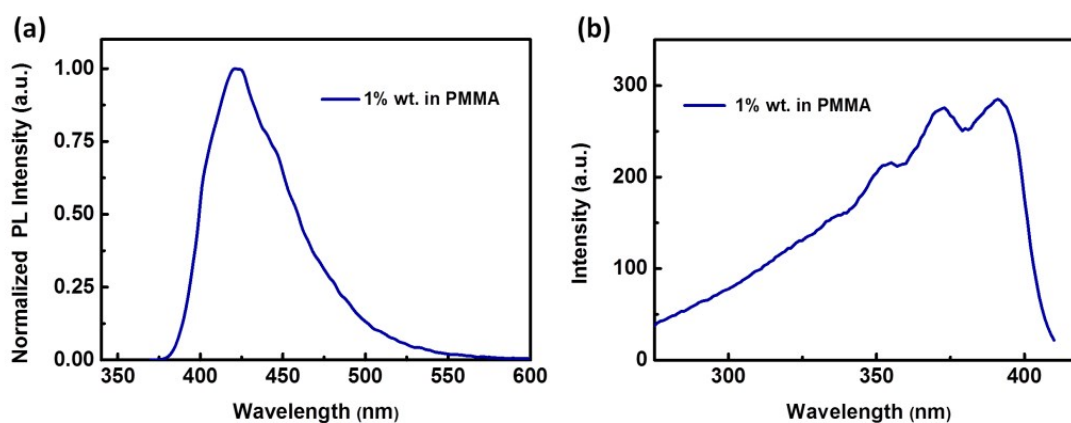


**Fig. S5** (a) The PL spectrum of mTPA-9-AN of 1% wt. in polymethylmethacrylate (PMMA). (b) The excitation spectrum of mTPA-9-AN of 1% wt. in PMMA, which was recorded at 421nm.

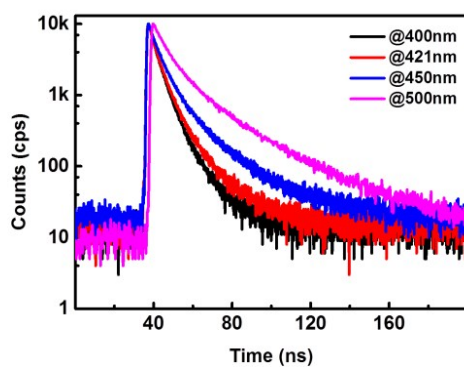


**Fig. S6** The lifetimes of mTPA-9-AN of 1% wt. in PMMA. They were recorded at different wavelength.

**Table S2.** The lifetimes of mTPA-9-AN of 1% wt. in PMMA at different wavelength

Wavelength (nm)	$\tau_1$ (ns)	$\tau_2$ (ns)
400	3.91 (69.50%)	9.89 (30.50%)
421	4.12 (67.72%)	12.10 (32.28%)
450	5.07 (61.34%)	17.67 (38.66%)
500	7.58 (54.99%)	29.82 (45.01%)

### 2.3 Crystal characters

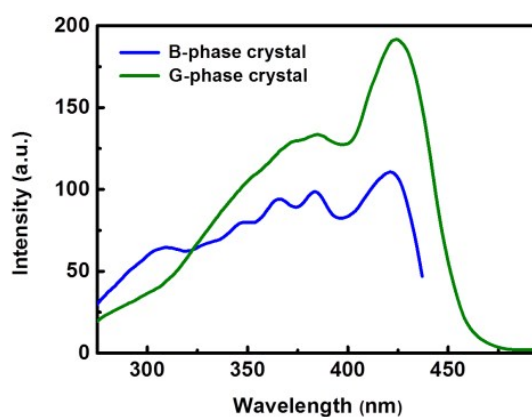
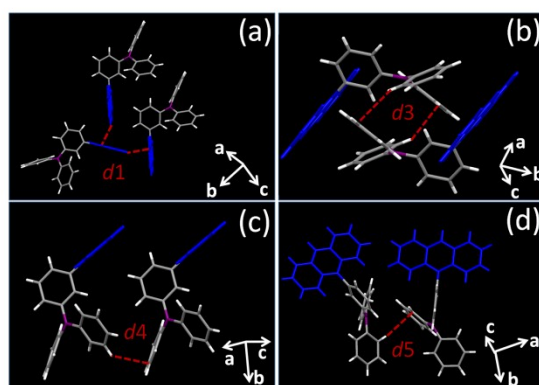


**Fig. S7** The excitation spectra of B-phase and G-phase crystals, which were recorded at 455 nm and 507 nm, respectively.

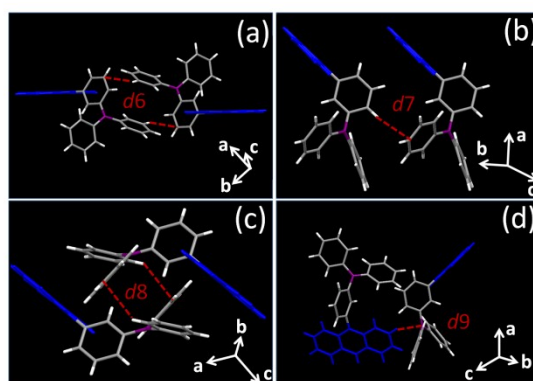


**Table S3.** Crystallographic data and structure refinements of B-phase and G-phase crystals

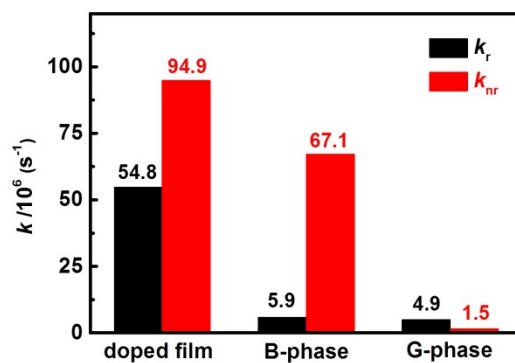
	B-phase crystal	G-phase crystal
crystal color	colorless	yellowish-green
empirical formula	C <sub>32</sub> H <sub>23</sub> N	C <sub>32</sub> H <sub>23</sub> N
formula weight	421.51	421.51
<i>T</i> [K]	296(2)	293(2)
crystal system	Orthorhombic	Monoclinic
space group	P ccn	P 21/n
<i>a</i> [Å]	18.1663(17)	14.901(3)
<i>b</i> [Å]	29.653(3)	8.3206(17)
<i>c</i> [Å]	8.5668(8)	18.900(4)
$\alpha$ [°]	90	90
$\beta$ [°]	90	101
$\gamma$ [°]	90	90
<i>V</i> [Å <sup>3</sup> ]	4614.9(8)	2297.0(8)
<i>Z</i>	8	4
<i>F</i> (000)	1776	888
density [g/cm <sup>3</sup> ]	1.213	1.219
$\mu$ [mm <sup>-1</sup> ]	0.070	0.070
reflections collected	32058	21529
unique reflections	5743	5248
<i>R</i> (int)	0.0886	0.0347
GOF	0.967	1.034
<i>R</i> <sub>1</sub> [ <i>I</i> > 2 $\sigma$ ( <i>I</i> )]	0.0540	0.0430
$\omega R_2$ [ <i>I</i> > 2 $\sigma$ ( <i>I</i> )]	0.1162	0.1246
<i>R</i> <sub>1</sub> (all data)	0.1399	0.0661
$\omega R_2$ (all data)	0.1648	0.1412



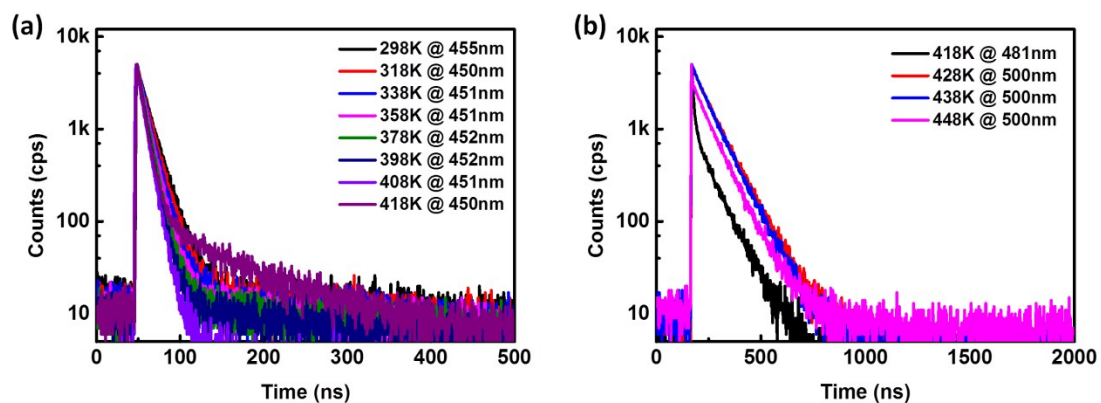
**Fig. S8** Stacking structure of B-phase crystal ( $d_1 = 2.817$  Å,  $d_3 = 2.783$  Å,  $d_4 = 2.834$  Å,  $d_5 = 2.853$  Å).



**Fig. S9** Stacking structure of G-phase crystal ( $d_6 = 2.819 \text{ \AA}$ ,  $d_7 = 2.845 \text{ \AA}$ ,  $d_8 = 2.900 \text{ \AA}$ ,  $d_9 = 2.814 \text{ \AA}$ ).



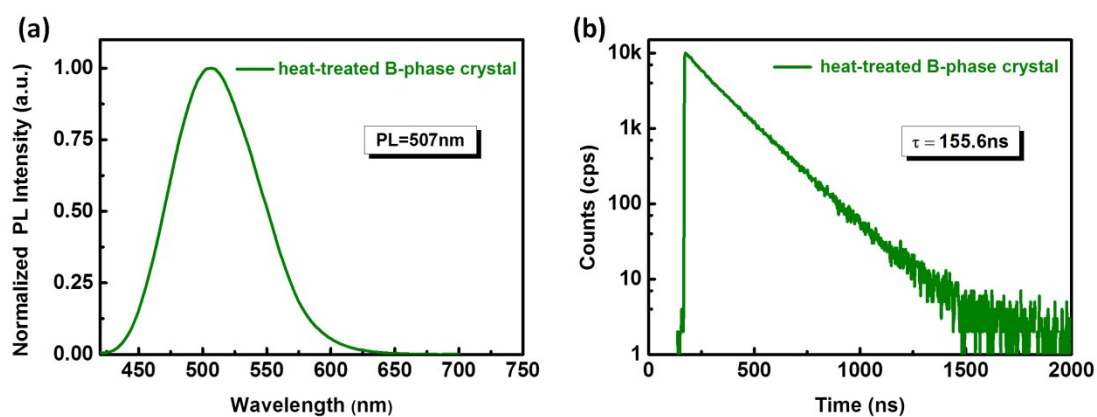
**Fig. S10** The  $k_r$  and  $k_{nr}$  of doped film, B-phase and G-phase crystals.



**Fig. S11** The lifetimes of B-phase crystal at different temperature.

**Table S4.** The lifetimes of B-phase crystal at different temperature

Temperature(K)	$\tau_1$ (ns)	$\tau_2$ (ns)
298	13.74	---
318	12.52	---
338	11.33	---
358	10.35	---
378	9.15	---
398	8.56	---
408	7.74(95.52%)	24.32(4.48%)
418 @450	7.47(77.58%)	88.13(22.42%)
@481	8.32(29.97%)	89.32(70.03%)
428	94.26	---
438	89.54	---
448	86.42	---

**Fig. S12** (a) The PL spectrum of heat-treated B-phase crystal at room temperature. (b) The lifetime of heat-treated B-phase crystal at room temperature, which was recorded at 507 nm. Both the wavelength and lifetime were consistent with those of G-phase crystal.

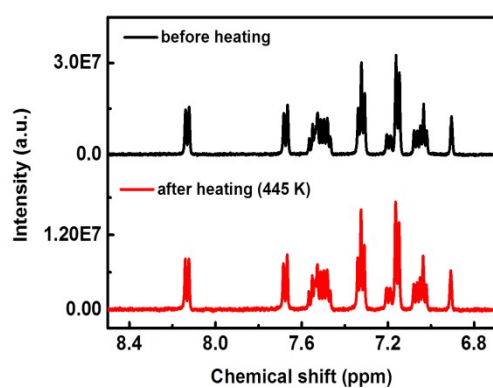


**Fig. S13**  $^1\text{H}$  NMR spectra of B-phase crystal before and after annealing.

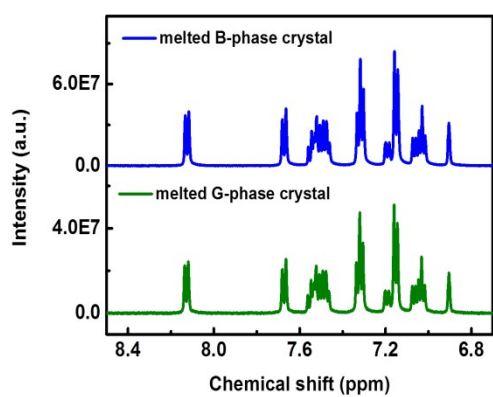


**Fig. S14**  $^1\text{H}$  NMR spectra of melted B-phase and G-phase crystals.

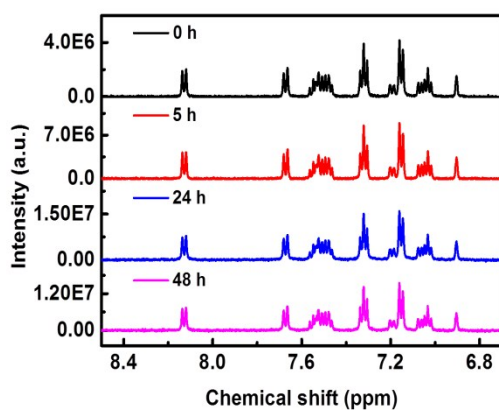


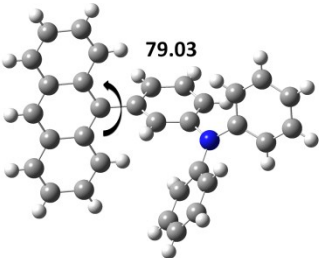
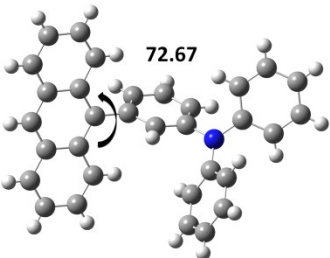
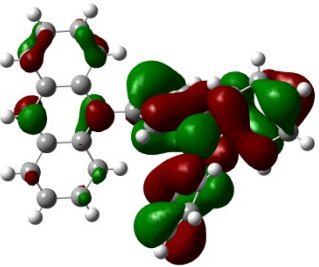
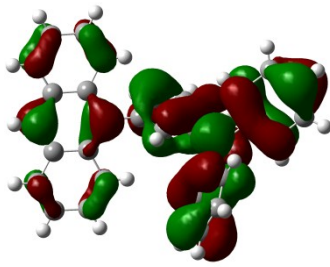
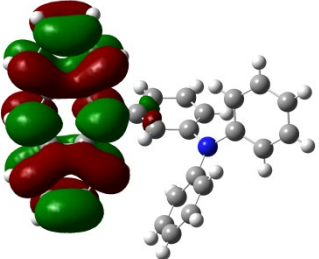
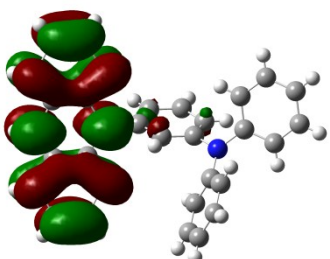
**Fig. S15**  $^1\text{H}$  NMR spectra of G-phase crystal after different UV-irradiation time.

### **3. Theoretical calculations**

To shed more light on the characters of monomer and dimer of mTPA-9-AN, density functional theory (DFT) and time-dependent density functional theory (TD-DFT) calculations were used to describe the ground-state and excited-state properties. Natural transition orbitals (NTOs) were evaluated with the dominant “particle”-“hole” pair contributions and the associated transition weights. All the calculations were carried out using Gaussian-09 package.

#### **3.1 Monomer characters**

The geometries of the ground state monomers were chosen from the B- and G-phase crystal, respectively. Such large twist angles completely break molecular conjugation between donor (TPA) and acceptor (AN). The highest occupied molecular orbital (HOMO) and the lowest unoccupied molecular orbital (LUMO) are mainly localized on the TPA and AN moieties, respectively (Figure S14). Such a large separation of HOMO and LUMO distributions is a typical characteristic of CT molecule, and is further confirmed by the solvatochromic spectra.

	B-phase monomer	G-phase monomer
Geometry		
HOMO		
LUMO		

**Fig. S16** Ground state geometries of monomers and frontier orbitals respectively.

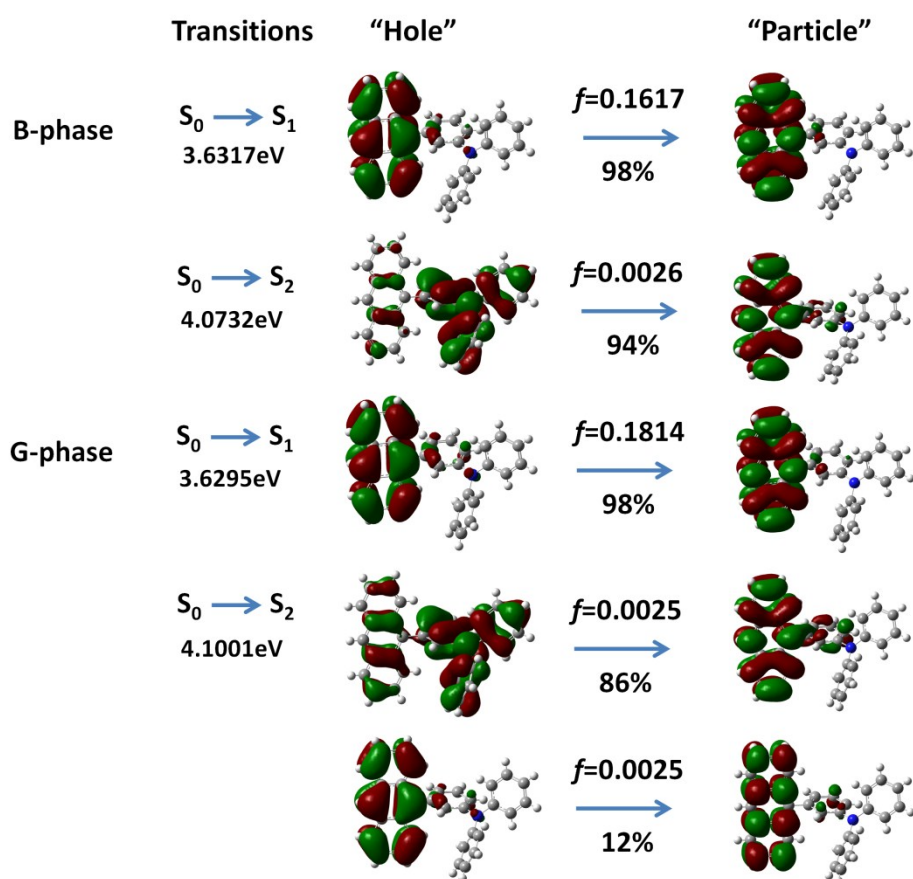
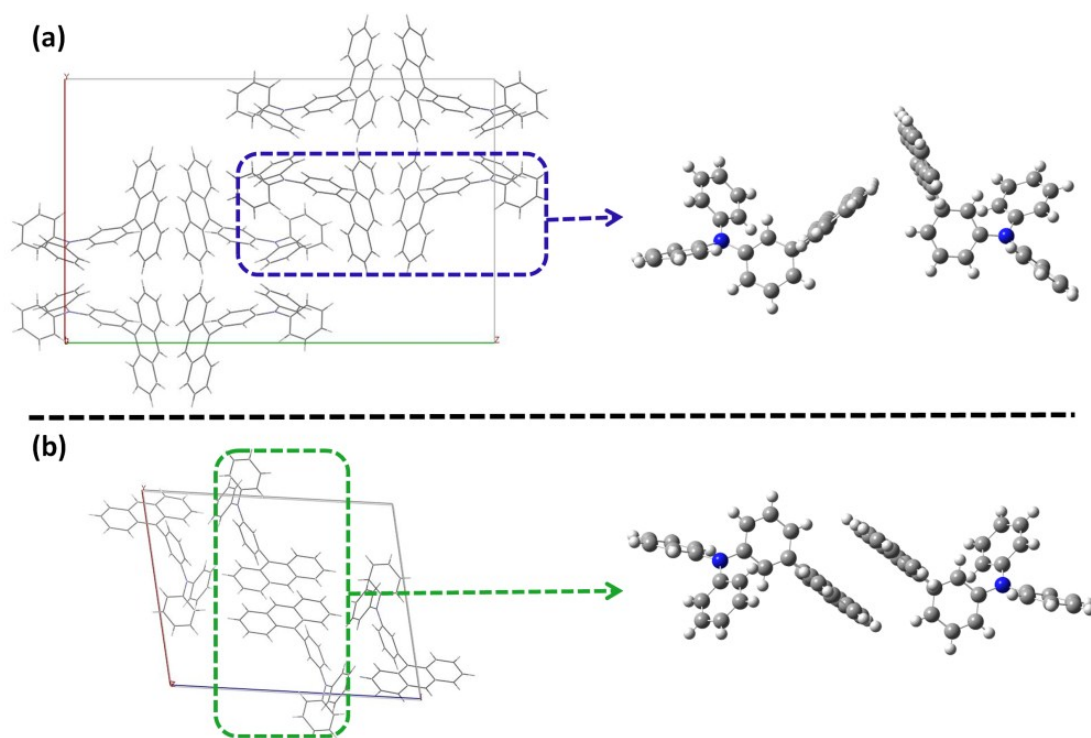


Fig. S17 NTOs of monomers.

### 3.2 Dimer characters

The geometries of the ground state dimer were selected from the B- and G-phase crystal in corresponding unit cell (Figure S16). Single point energy and excited state geometries of  $\pi$ - $\pi$  stacking dimer were obtained by using the M06-2X hybrid functional at 6-31G (d, p) level. As for the transition density matrix color-filled maps, labels in abscissa and ordinate correspond to indices of heavy atoms. Figure S19 shows the correspondence between labels and atoms. We ordered the atoms by labeling TPA segment first and then the AN segment. Since hydrogen atoms usually

have little contribution to the transition we are interested in, they are usually ignored by default.



**Fig. S18** The configuration of (a) B-phase dimer, and (b) G-phase dimer.

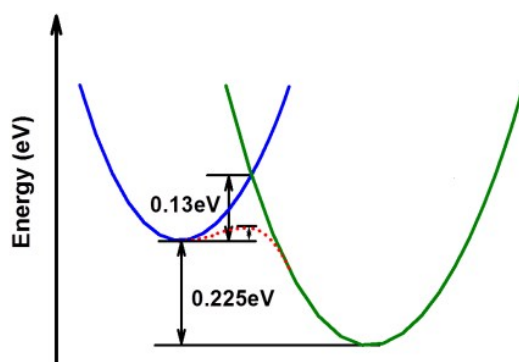


**Fig. S19** Schematic diagram of potential energy surfaces of B-phase and G-phase dimer.



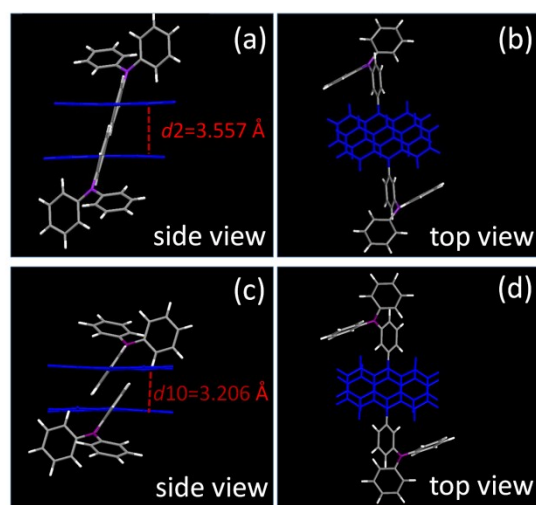


**Fig. S20** The geometries of (a), (b) ground state and (c), (d) excited state.

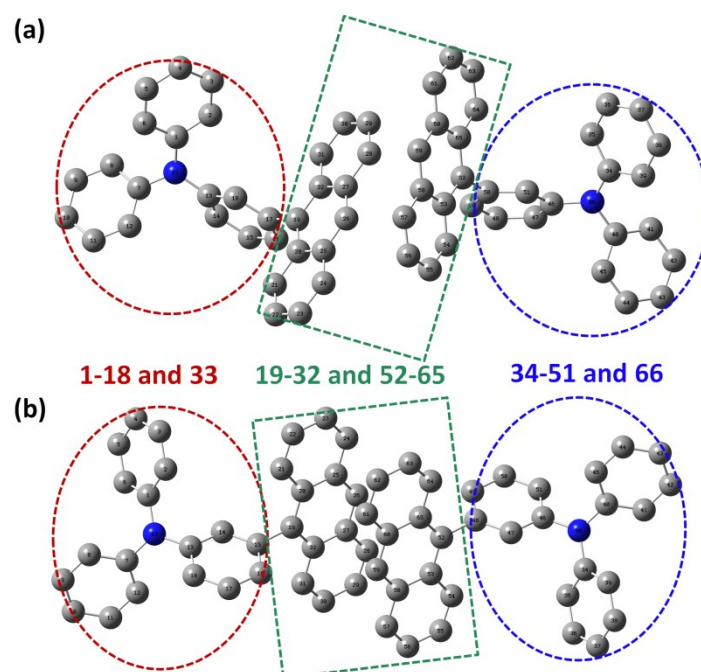


**Fig. S21** The labels of atoms (a) B-phase dimer (b) G-phase dimer.

#### 4. Photophysical properties of TPA-AN

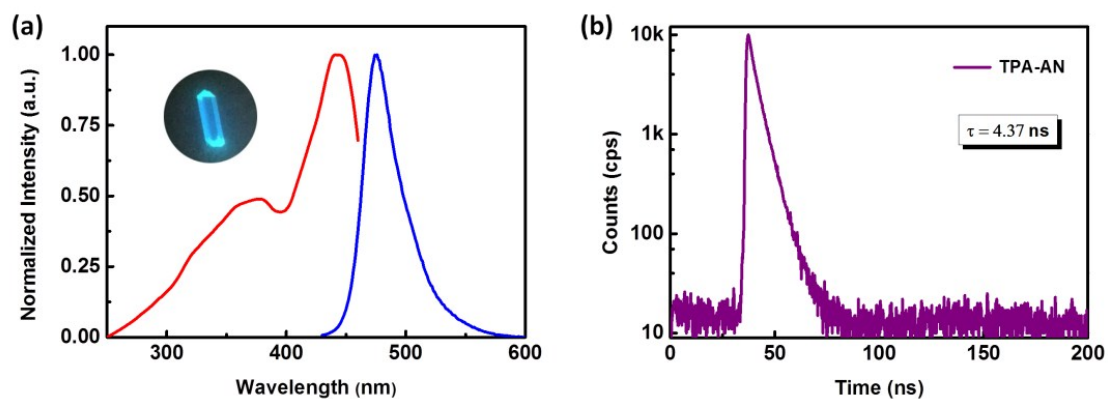


**Fig. S22** The spectra of TPA-AN crystal (a) Excitation (red), PL (blue) spectra and the photograph under UV light (365 nm). (b) Transient PL spectrum. The excitation and transient PL spectra were obtained by monitoring at 476 nm, and the PL spectrum was obtained by excitation at 415 nm.